Bioinspiration & Biomimetics

PAPER

A computational model of insect campaniform sensilla predicts encoding of forces during walking

To cite this article: Nicholas S Szczecinski *et al* 2021 *Bioinspir. Biomim.* **16** 065001

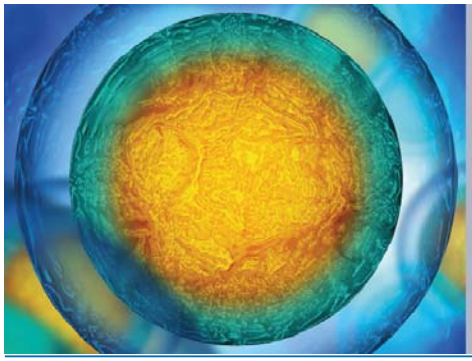

Bioinspiration & Biomimetics

PAPER

RECEIVED
31 March 2021

REVISED
21 June 2021

ACCEPTED FOR PUBLICATION
12 August 2021

PUBLISHED
7 September 2021

A computational model of insect campaniform sensilla predicts encoding of forces during walking

Nicholas S Szczecinski[1,*], Chris J Dallmann[2], Roger D Quinn[3] and Sasha N Zill[4]

[1] Department of Mechanical and Aerospace Engineering, West Virginia University, Morgantown, WV 26505, United States of America
[2] Department of Physiology and Biophysics, University of Washington, Seattle, WA 98195, United States of America
[3] Department of Mechanical and Aerospace Engineering, Case Western Reserve University, Cleveland, OH 44106, United States of America
[4] Department of Biomedical Sciences, Joan C Edwards School of Medicine, Marshall University, Huntington, WV 25755, United States of America
[*] Author to whom any correspondence should be addressed.

E-mail: nicholas.szczecinski@mail.wvu.edu

Keywords: campaniform sensilla, sensory feedback, adaptation, hysteresis, yank, power law

Supplementary material for this article is available online

Abstract

Control of forces is essential in both animals and walking machines. Insects measure forces as strains in their exoskeletons via campaniform sensilla (CS). Deformations of cuticular caps embedded in the exoskeleton excite afferents that project to the central nervous system. CS afferent firing frequency (i.e. 'discharge') is highly dynamic, correlating with the rate of change of the force. Discharges adapt over time to tonic forces and exhibit hysteresis during cyclic loading.

In this study we characterized a phenomenological model that predicts CS discharge, in which discharge is proportional to the instantaneous stimulus force relative to an adaptive variable. In contrast to previous studies of sensory adaptation, our model (1) is nonlinear and (2) reproduces the characteristic power-law adaptation with first order dynamics only (i.e. no 'fractional derivatives' are required to explain dynamics). We solve the response of the system analytically in multiple cases and use these solutions to derive the dynamics of the adaptive variable. We show that the model can reproduce responses of insect CS to many different force stimuli after being tuned to reproduce only one response, suggesting that the model captures the underlying dynamics of the system. We show that adaptation to tonic forces, rate-sensitivity, and hysteresis are different manifestations of the same underlying mechanism: the adaptive variable. We tune the model to replicate the dynamics of three different CS groups from two insects (cockroach and stick insect), demonstrating that it is generalizable. We also invert the model to estimate the stimulus force given the discharge recording from the animal. We discuss the adaptive neural and mechanical processes that the model may mimic and the model's use for understanding the role of load feedback in insect motor control. A preliminary model and results were previously published in the proceedings of the Conference on Biohybrid and Biomimetic Systems.

1. Introduction

Campaniform sensilla (CS) are strain-sensitive mechanoreceptors in the exoskeleton of insects (Chapman *et al* 1973, Zill and Moran 1981a, Harris *et al* 2020). Each sensillum consists of a cap in the cuticle that when compressed, mechanically distorts a sensory neuron's dendrite and causes the afferent to fire action potentials (APs) (figure 1(a)). Because the strain of a body is proportional to the stress within it, CS can function as force- or load-sensing organs (Ridgel *et al* 1999, Kaliyamoorthy *et al* 2005, Zill *et al* 2011). CS are found wherever an insect's body experiences significant strain during behavior, including on the legs (Harris *et al* 2020), on the antennae (Mongeau *et al* 2015), and across wings and halteres (Agrawal *et al* 2017, Dickerson *et al* 2021).

Insects control their leg posture and locomotion using load feedback from CS (Zill *et al* 2004, Tuthill and Wilson 2016, Dickerson *et al* 2021), similarly to the way vertebrates use load feedback from Golgi tendon organs (Jami 1992, Prochazka *et al* 1997a, 1997b, Duysens *et al* 2000). For example, feedback from leg CS is thought to reinforce muscle activity

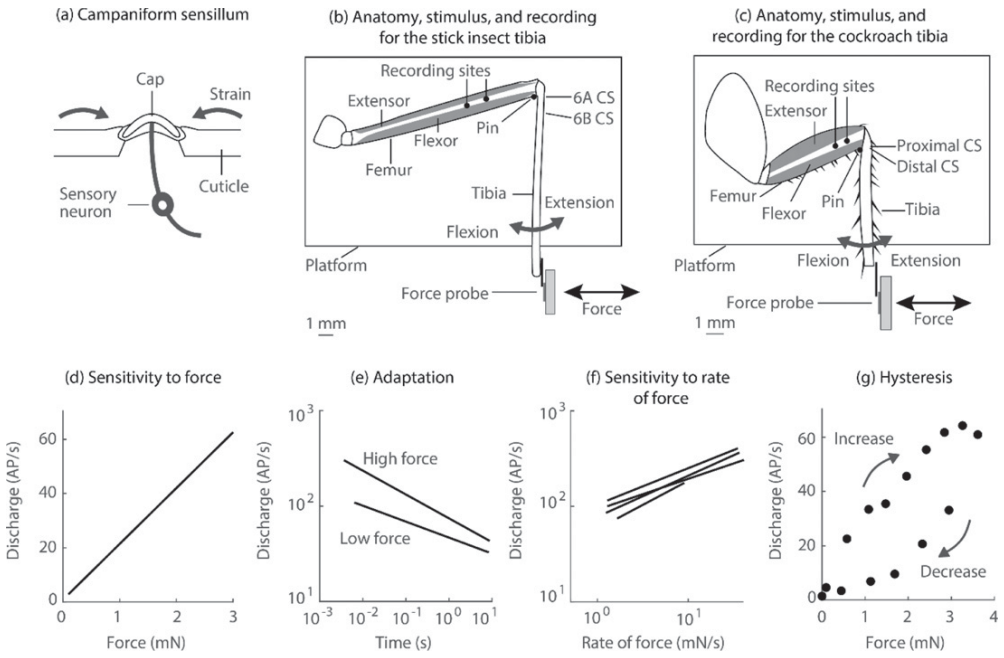

Figure 1. (a) Schematic of a campaniform sensillum (CS), illustrating how the cap is deformed by bending moments that compress the cuticle. The cap's deflection strains a sensory neuron's dendrite, causing it to discharge APs. (b) Schematic of the stick insect leg with recording sites, muscle groups in the femur that actuate the tibia, and tibial CS groups labeled (insect body not shown). Schematic also illustrates the experimental setup. Animals were fixed to a platform with staples. Movements of the FTi joint were prevented by a pin glued to the proximal end of the tibia. Force was applied by a probe equipped with strain gauges and actuated by a DC motor. (c) Experimental set up for recording from CS of the cockroach leg (similar to (b)). (d) Experimental data characterizing response properties of CS afferents (Ridgel *et al* 2000) that support the assumptions of the model: discharge (APs per second) is proportional to load, with a small offset; (e) peak discharge during a ramp stimulus is proportional to the rate of load, with a power-law relation; (f) discharge rate decays over time according to a power-law; and (g) discharge exhibits hysteresis under repeated loading. Reprinted by permission from Springer Nature Customer Service Centre GmbH: Springer Nature, Journal of Comparative Physiology A [Ridgel *et al.*] (c) 2000.

during the stance phase of walking (Pearson 1972, Zill *et al* 2015) and contribute to inter-leg coordination (Zill *et al* 2009, Dallmann *et al* 2017). Such pathways appear particularly important during slow walking due to the latency between CS discharge and subsequent motor neuron activation (Zill and Moran 1981b). Despite the apparent importance of CS feedback during walking, it remains largely unknown precisely how feedback from CS is integrated to control the body, partly due to the technical difficulty of targeted experimental manipulations and recordings during natural behavior.

Mathematical and robotic models of animal locomotion are powerful tools with which to address the question of how load feedback is used in body control. In such models, feedback can be manipulated at will, enabling one to test the necessity and sufficiency of specific sensory feedback to perform control tasks (Prochazka and Gorassini 1998, Elzinga *et al* 2012, Chung *et al* 2015, Markin *et al* 2016, Naris *et al* 2020). However, to provide meaningful insights into control, the dynamics of sensory feedback must be modeled realistically. CS are not simple sensors that directly report the forces experienced by the leg to the nervous system. Instead, they have a complicated dynamic response to load (Ridgel *et al* 2000, Zill *et al* 2011, Zill *et al* 2018): CS discharge adapts rapidly over time in response to tonic forces and is completely silenced by decreasing forces; CS discharge primarily reflects the positive rate of change of force, but with a power-law scaling; CS discharge exhibits hysteresis, wherein the afferent firing reflects both the instantaneous and past load imposed on the CS. To better understand the functional role of load feedback in posture and locomotion, a mathematical model is needed that can relate recordings of CS discharge to the forces acting on the leg (Goldsmith *et al* 2020).

Mathematical models have been formulated to describe the afferent firing of CS (Chapman *et al* 1979, Szczecinski *et al* 2020), other load sensors such as spider slit sensilla (Torkkeli and French 2002) and vertebrate Golgi tendon organs (Prochazka and Gorassini 1998). Models have also been developed for other sensory afferents (Dallmann *et al* 2021), including insect hair fields (Ache and Dürr 2015), insect cerci (Chapman and Smith 1963), insect photoreceptors (Thorson and Biederman-Thorson 1974), vertebrate muscle spindles (Prochazka and Gorassini 1998, Blum *et al* 2020), and others. All these sensory systems show adaptation in neural activity in response to tonic inputs (French 1984). A particularly intriguing property of many of these afferents is that they adapt to tonic inputs according to a power-law over time, e.g. $y = a \cdot t^k$, where y is the sensory discharge,

Table 1. List of abbreviations.

Abbreviation	Definition
$\boldsymbol{A}$	Amplitude of bending force stimulus in millinewtons
AP	Action potential
CS	Campaniform sensillum/sensilla
FTi	Femur-tibia joint
GA	Genetic algorithm
MAE	Mean absolute error
N	Number of individual animals used in an experiment
n	Number of total trials conducted for an experiment
$\boldsymbol{T}$	Duration of ramp phase of bending force stimulus in seconds
$\boldsymbol{u}$	Stimulus force applied to the tibia in millinewtons
$\boldsymbol{x}$	Model's dynamic variable
$\boldsymbol{y}$	Model discharge in APs per second

t is time, k is a constant exponent, and a is a constant multiplier (Thorson and Biederman-Thorson 1974, French and Torkkeli 2008). This is surprising because it suggests underlying dynamics quite different from typical engineered systems. For example, many engineered control systems cause adaptation according to an exponential function over time, e.g. $y = a \cdot \exp\left(-t/\tau\right)$ which is the solution to a linear first-order differential equation with time constant τ. However, the power-law adaptation $y = a \cdot t^k$ is the solution to a kth-order differential equation, that is, a system whose dynamics include fractional (i.e. non-integer) derivatives of its states (French 1984). While such an insight is a valuable description, it is not clear what chemical, electrical, or mechanical mechanism may compute the fractional derivative of a stimulus (Thorson and Biederman-Thorson 1974, Di Paola *et al* 2013). One motivation for the present study is to formulate an integer-order dynamical model that also produces power-law decay over time. An integer-order model may have more intuitive physical meaning and be simpler to implement for simulation or data filtering on board a robot.

Here we describe and analyze a nonlinear model that does not rely on fractional derivatives to produce power-law adaptation over time. Conceptually, the model is simple: the discharge frequency is proportional to the stimulus force, relative to a nonlinear adaptive variable (see table 1 for a list of variables and their meanings). This nonlinear formulation does not allow the application of linear analysis, which is possible for fractional derivative formulations (Chapman and Smith 1963). However, since it is a first order (i.e. not fractional order) system, its dynamics could describe several neural or mechanical phenomena, such as slow sodium channel inactivation in receptor cells (Torkkeli and French 2002) or the viscoelastic straining of body tissues (Brown and Stein 1966, Hillerton 1984). Furthermore, our analysis directly links the form of power-law adaptation to the structure of the model, such that the model parameters dictate the shape of the responses. However, despite the similarity to multiple adaptive mechanisms, the model is phenomenological in that it reproduces the input-output relationship of CS afferents without specifically modeling any particular mechanism(s). The advantages of such an abstract, phenomenological model is its compactness and computational efficiency, which facilitate its integration within a multi-scale model of the motor system (Markin *et al* 2016, Prilutsky *et al* 2016, Goldsmith *et al* 2020, Sandbrink *et al* 2020, Dallmann *et al* 2021).

In this manuscript we show that our simple phenomenological model reproduces the responses of cockroach and stick insect tibial CS with minimal parameter tuning. We show that all dynamic response properties, i.e. adaptation, rate-sensitivity, and hysteresis, emerge from the model's one basic underlying mechanism: computing the discharge as the instantaneous load relative to a dynamic adapting variable. We derive the first-order, nonlinear system that produces power-law adaptation. We show how such a model approximates rate-sensitivity, indicating that the adaptation and rate-sensitivity are linked. If we eliminate the adapting variable, then hysteresis disappears, demonstrating that the adapting variable and hysteresis are linked. Having established the model's gross response properties, we then show that the model can reproduce CS discharges in response to highly dynamic force stimuli which it has not been tuned to reproduce. We show that the model can be inverted, enabling the estimation of highly dynamic forces acting on the leg based on CS afferent recording alone. Throughout the study, we compare the model's accuracy to a fractional-derivative model and show that the former replicates discharge more accurately than the latter in most of the cases tested. In the discussion, we relate our model to previous models, discuss our model's applications to CS and other sensory systems, and discuss its application to simulation and robotics.

2. Methods

2.1. Recordings of campaniform sensilla discharge

Sensory discharges from the tibial CS of the American cockroach (*Periplaneta americana*) and Indian stick

Table 2. Parameter values used in this study. Values for the cockroach proximal tibial group were calculated by minimizing the mean squared error between the response to the ramp-and-hold stimulus depicted in figure 3(a) and the model's response to the same stimulus. Values for the stick insect group 6A were found by minimizing the mean squared error between the recorded 6A discharge depicted in figure 7(a) and the model's response to the same stimulus. Values for the stick insect group 6B were found by minimizing the mean squared error between the recorded 6B discharge depicted in figure 7(b) and the model's response to the same stimulus.

Group	Cockroach Prox. tibia	Stick insect 6A	Stick insect 6B
Amplitude of adaptive term, $\boldsymbol{a}$ (Hz mN^{-1})	707.6	265.0	605.0
Exponent of adaptive term, $\boldsymbol{b}$ (unitless)	2.262	1.675	3.325
Amplitude of proportional term, $\boldsymbol{c}$ (Hz mN^{-1})	54.29	17.75	5.750
Amplitude of bias term, $\boldsymbol{d}$ (Hz)	−41.16	−22.50	10.50
Amplitude of adaptive time constant, $\boldsymbol{\tau}$ (ms)	3.859	9.678	1.659
Figures using this instance of the model	2, 3, 4, 5, 8	6, 10	6, 7, 9, 10
Model tuned using single trial from figure	3(a)	7(a)	7(b)

insect (*Carausius morosus*) were recorded extracellularly. Methods for recording from the CS have been described in detail (cockroach: (Ridgel *et al* 2000); stick insect: (Zill *et al* 2011)) and are briefly described below (figures 1(b) and (c)). For both species, the abdomen, thorax, and proximal leg segments of each animal were restrained by staples. The femur-tibia (FTi) joint was paralyzed by cutting the nerves that supply the femoral muscles. A pin was placed adjacent to proximal end of the tibia and a small drop of cyanoacrylate glue was applied to link the pin and tibia and prevent rotation. The pin was positioned such that the tibial CS were distal to this anchor point. CS normally respond to loads that are resisted by muscle contractions. In the experimental arrangement, externally imposed forces and moments were counteracted instead by the glued pin. The tarsus was then ablated. Force waveforms generated by an analog to digital interface (Spike 2, Cambridge Electronics) were applied to the distal end of the tibia by a probe actuated by a DC motor. The resultant forces were measured via strain gauges within the probe.

To extracellularly record APs from CS afferents, silver wires were inserted in the femur near nerves that carry afferents from the tibial CS. APs were identified in recordings based on thresholding and treated as discrete events. The source of each AP (i.e. which CS group) was determined by AP amplitude, direct cap stimulation, and cap ablation (Ridgel *et al* 2000). A continuous discharge rate (AP/s) was calculated by counting the number of AP events that took place within a moving window of time (typically 20 ms).

2.2. Features of campaniform sensilla discharge

CS discharge is highly dynamic and reflects multiple features of the stimulus force. The plots in figures 1(d)–(g) summarize characterization of CS discharge dynamics reported in (Ridgel *et al* 2000). CS discharge in response to a tonic stimulus is proportional to the amplitude of the stimulus (figure 1(d)). When the stimulus level changes, the discharge adapts to the new level of force according to a power-law function of time (i.e. the discharge $y(t) \propto t^{k_2}$, figure 1(e)). CS discharge in response to a phasic stimulus reflects the rate of change of the stimulus according to a power-law relationship (i.e. the discharge $y \propto \left(\frac{du}{dt}\right)^{k_1}$, where u is the stimulus force and k_1 is the slope of the line of best fit on logarithmic axes, figure 1(f)). Finally, the discharge in response to a stimulus depends on whether the stimulus increased or decreased to that level (figure 1(g)). CS responses to these simple stimuli (i.e. ramp-and-hold) were used to produce a dynamic, phenomenological model of CS discharge that captures responses to highly dynamic stimuli and can be inverted to predict what forces cause recorded CS discharge patterns.

2.3. Dynamic phenomenological model of campaniform sensilla discharge

Considering the features of CS discharge described in the previous section, a continuous dynamical description of the discharge rate, y, was formulated. Because y represents a firing rate, it must be positive. When subjected to a tonic stimulus, y is proportional to the stimulus force u plus a constant bias (Ridgel *et al* 2000, Zill *et al* 2011), meaning that y should include $c \cdot u + d$, where c and d are constant parameters. Finally, it is known that y reflects $\dot{u}$, the rate of change of u; y adapts to tonic u according to a power-law function over time; and y exhibits hysteresis as u oscillates. We hypothesized that all three of these features, i.e. rate-sensitivity, power-law adaptation, and hysteresis, would emerge from a single term in the model, $a \cdot (u - x)$. This term is the difference between the stimulus u and a slowly adapting variable, x. The resulting model is:

$$y = \max\left(0, a \cdot (u - x) + c \cdot u + d\right) \tag{1}$$

$$\tau \cdot \dot{x} = f\left(u - x\right), \tag{2}$$

where a, c, d, and τ are constant parameters (see table 2) and f is a scalar valued function that increases

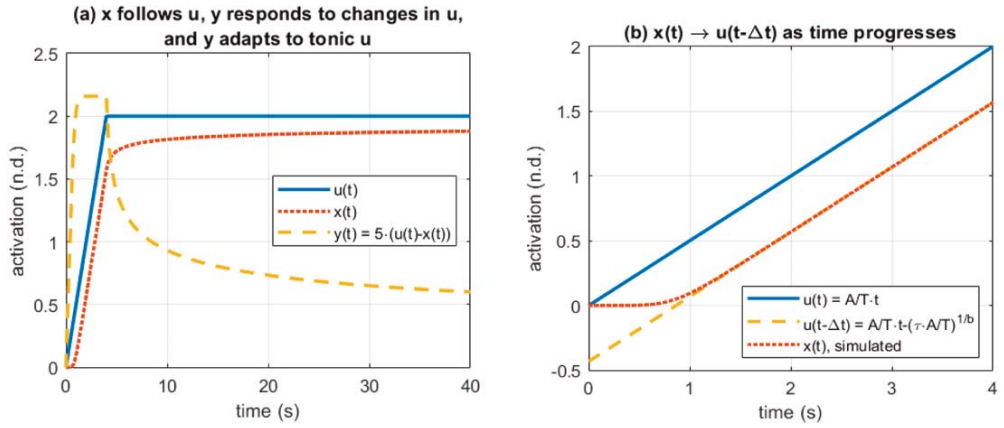

Figure 2. Basic behavior of the model. (a) The model response can be described by three key ideas: x follows the value of u, albeit by a nonlinear function; y peaks while u is increasing, approximating the rate of change of u; and y adapts to 0 when u is constant. (b) The steady-state response of x is a time-delayed version of u when u is a ramp function. The input ramp, $u(t)$, is plotted in solid blue; the input ramp delayed by Δt is plotted in dashed yellow; the full simulated response $x(t)$ is plotted in dotted red. The dotted red curve approaches the dashed yellow curve over time. In this plot, $A = 2, T = 4, b = 5, \tau = 30 \times 10^{-3}$, and the resulting time shift from equation (18) is $\Delta t = 0.8635$ s.

monotonically and satisfies $f(0) = 0$. Due to these requirements on f, the only equilibrium value for x is $x = u$, which occurs after enough time has elapsed. Thus, the $a \cdot (u - x)$ term causes the value of y to adapt to a tonic force: as time elapses, x approaches u, causing y to decrease until $y = c \cdot u + d$ (figure 2(a)).

How does y reflect $\dot{u}$ if there is no $\dot{u}$ term in equation (1)? We observe that when u is a ramp function of the form $A/T \cdot t$, the steady-state response of x is the same as u, but delayed by time Δt (figure 2(b)). This means that in steady-state, the first term in equation (1), $a \cdot (u - x) = a \cdot (u(t) - u(t - \Delta t))$. If $a = 1/\Delta t$, then this term would be the finite-difference approximation of $\dot{u}$. Thus, the adaptation term in the model directly endows it with rate-sensitivity. We show in the results that eliminating this term also eliminates hysteresis in the model, demonstrating that adaptation, rate-sensitivity, and hysteresis are all linked.

What is the form of f? Because CS discharge adapts to tonic inputs according to a power-law over time (i.e. $y = A \cdot t^k$ (Ridgel *et al* 2000), we seek a function f such that $y_{ss} = a \cdot (u - x_{ss}) \propto \dot{u}^k$, where x_{ss} is the steady-state response of x, y_{ss} is the steady-state response of y, and k is a constant coefficient. To determine the form of f, we calculated the response of y to a ramp input of the form $u = \frac{A}{T} \cdot t$, where t is time and A and T are constants that determine the slope of the ramp. From simulation (figure 2(b)), we observed that x_{ss} lags u by Δt,

$$x_{ss} = u(t - \Delta t) = \frac{A}{T} \cdot (t - \Delta t), \tag{3}$$

where Δt is to be determined. We observed that the corresponding steady-state response of y,

$$y_{ss} = a \cdot (u(t) - u(t - \Delta t)), \tag{4}$$

would be the finite-different approximation of $\dot{u}$ if $a = \frac{1}{\Delta t}$. Thus, y_{ss} approximates $\dot{u}$ without including an explicit $\dot{u}$ term in y.

Computing Δt in terms of the stimulus and model parameters set the form of the low-pass filter function f necessary to achieve the goal that $y_{ss} \propto \dot{u}^k$. To compute Δt, we substituted equation (3) into equation (2), recognized that $\dot{x}_{ss} = \frac{A}{T}$, and rearranged:

$$\Delta t = \frac{T}{A} \cdot f^{-1}\left(\tau \cdot \frac{A}{T}\right). \tag{5}$$

Substituting equation (5) into equation (4) and simplifying,

$$y_{ss} = a \cdot f^{-1}\left(\tau \cdot \frac{A}{T}\right). \tag{6}$$

Recall that when u is a ramp function, $\dot{u} = \frac{A}{T}$, so

$$y_{ss} = a \cdot f^{-1}(\tau \cdot \dot{u}). \tag{7}$$

Setting $f(z) = \text{sign}(z) \cdot |z|^b$ such that $b = \frac{1}{k}$ is a constant parameter accomplishes the goal of finding $f(z)$ such that $y \propto \dot{u}^k$. Thus,

$$f(u - x) = \text{sign}(u - x) \cdot |u - x|^b. \tag{8}$$

2.4. Derivation of the model's step response

Experimental data shows that discharge frequency adapts according to a power law function of time (Chapman and Smith 1963, Ridgel *et al* 2000, French and Torkkeli 2008). Here we demonstrate that our model replicates this behavior. Consider the first-order nonlinear system from equations (1) and (2) written to explicitly include the form of f from equation (8):

$$\tau \cdot \dot{x} = \text{sign}(u - x) \cdot |u - x|^b \tag{9}$$

$$y = a \cdot (u - x)\,. \tag{10}$$

We sought to show that when $x\,(t = 0) = x_0$ and $u = 0$, x approaches 0 according to a power-law function of time,

$$x\,(t) = B \cdot \left(\frac{\mathrm{t} + \Delta t}{\tau}\right)^{s}, \tag{11}$$

where B, s, and Δt are constant coefficients. We required that $s < 0$ to ensure that the response decays over time and that $\Delta t > 0$ to avoid a singularity when $t = 0$. We also assumed that sign $(B) = \mathrm{sign}(x_0)$. We solved for B and s by the 'lucky guess' method, substituting equation (11) and its time derivative into equation (9). The time derivative of equation (11) is:

$$\dot{x}\,(t) = \frac{B \cdot s}{\tau} \cdot \left(\frac{t + \Delta t}{\tau}\right)^{s-1}. \tag{12}$$

Substituting equations (11) and (12) into equation (9), we obtained:

$$-B \cdot s \cdot \left(\frac{t + \Delta t}{\tau}\right)^{s-1} = B^b \cdot \left(\frac{t + \Delta t}{\tau}\right)^{s \cdot b}. \tag{13}$$

For the left- and right-hand sides to be equal for all times, both exponents must be equal and both coefficients of time must be equal,

$$s - 1 = s \cdot b, \tag{14}$$

$$-B \cdot s = B^b. \tag{15}$$

Rearranging equation (14) to solve for s, substituting the result into equation (15), and solving equation (15) for B yielded:

$$s = \frac{1}{1 - b}, \tag{16}$$

$$B = (b - 1)^{\frac{1}{1-b}}. \tag{17}$$

The final remaining constant Δt was calculated by substituting the initial condition $x\,(t = 0) = x_0$ into equation (11) and simplifying,

$$\Delta t = \tau \cdot \frac{x_0^{1-b}}{b - 1}. \tag{18}$$

That equations (16)–(18) can be solved indicates that equation (11) is indeed the transient solution of equation (9). Thus, we have accomplished the goal of demonstrating that our CS model will adapt to a tonic force according to a power-law over time, as determined experimentally. Furthermore, all three of the constant parameters in the solution, s, B, and Δt, can be expressed in terms of the constants τ and b from equation (9), meaning that the decay response can be computed directly and analytically as soon as the parameter values are set, without simulation.

2.5. Model parameter selection

The model's goal is to map from a time-varying force stimulus to a time-varying discharge frequency of the afferent. We call this the 'forward model', in which force stimulus is the input, and sensory discharge is the output. Data of this form represent a rate-coding of mechanical states. Many sensory neuroscience studies report data this way (Chapman and Smith 1963, Zill and Moran 1981a, Ridgel *et al* 2000), making it the simplest form the model could take.

We tuned multiple instances of the forward model to model the tibial CS of cockroaches (proximal group) and stick insects (groups 6A and 6B, figures 1(b) and (c)). To tune the cockroach proximal CS model, we used gradient-based optimization to minimize the mean-squared-error between the recorded discharge pattern (figure 3(a)) and the model's output, sampled at the same points in time. This is in effect a least-squared minimization problem (Dennis and Schnabel 1983). Due to the simplicity of the ramp-and-hold stimulus used to tune the model (shown in figure 3(a)), it was possible to estimate good starting values for the model parameters by hand. The parameters whose values were optimized, their descriptions, and their values are listed in table 2.

To tune the stick insect groups 6A and 6B models, the constant parameters were tuned by first using a genetic algorithm (GA) to minimize the mean-squared-error between the recorded discharge patterns and the model discharge (figures 7(a) and (b)), and then refining the GA's solution with gradient-based optimization as described in the previous paragraph. The GA was necessary to find good starting values for the parameters because it broadly explores the parameter space before converging on the values that provide the best solution (De Jong 1975). Our GA was greatly accelerated by establishing a grid of permissible parameter values, storing the mean-squared-error of each value combination in memory, and then skipping simulation if that value combination had already been evaluated. More details are provided in the supplementary materials (https://stacks.iop.org/BB/16/065001/mmedia). This discretized approach was sufficient because the GA's best solution was refined by more precise gradient-based minimization.

To compare the accuracy of our model to that of the fractional derivative approach, we applied these same tuning methods to tune the parameters in a fractional derivative model,

$$y = \max\left(0, a \cdot D^b u\,(t)\right), \tag{19}$$

where y is the instantaneous afferent discharge; a and b are constant parameters; and D is the derivative operator, such that D^b represents the bth derivative of the force stimulus, $u(t)$. Because the discharge is measured in APs per second, it must be positive. Fractional derivatives were calculated numerically with a Matlab toolbox (Jonathan 2021).

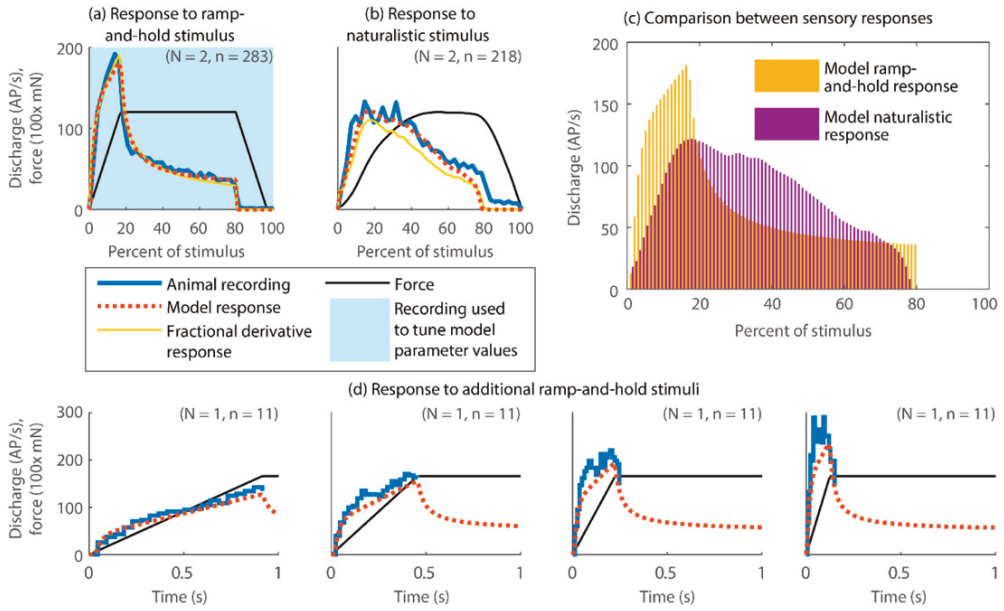

Figure 3. The dynamical model captured the discharge dynamics of CS in response to loading. (a) The discharge in response to a single ramp-and-hold waveform, measured in APs per second (AP/s), was used to tune model parameters. This demonstrates that the model can capture the basic discharge pattern of CS. The duration of the recording is 0.8 s. (b) Without retuning parameter values, the model replicated the CS discharge pattern in response to a dynamic joint torque waveform (from (Dallmann *et al* 2016)). The duration of the recording is 0.8 s. (c) When compared, the model's discharge in response to these two waveforms differed as seen in the animal (Zill *et al* 2018): the response to the ramp-and-hold had a higher peak and adapted more quickly, while the response to the naturalistic torque was relatively 'flat' and adapted slowly. (d) Sampling of CS discharges at high resolution during ramps of different rates. Afferent frequency reflected the amplitude of force at slow rates but increasingly indicated dF/dt in more rapid ramps. Without retuning, the model captured the discharge in response to ramp stimuli of increasing rate, suggesting that the model captures the underlying dynamics of CS discharge. Reprinted by permission from Springer Nature Customer Service Centre GmbH: Springer Nature, Conference on Biomimetic and Biohybrid Systems [Szczecinski *et al.*] (c) 2020.

2.6. Model inversion: one-group technique

The model described so far is a forward model (i.e. force stimulus in, sensory discharge out). The forward model may be 'inverted', in which the input is an afferent discharge recording and the model outputs the stimulus force required to generate the response. Although CS groups frequently exist in 'antagonistic' pairs that encode bending forces in opposing directions (Ridgel *et al* 1999, Zill *et al* 2012), CS responses are often experimentally characterized by unidirectional forces that primarily activate one CS group. This is justified because studies that have measured limb segments forces during walking show that some segments experience unidirectional forces, e.g. the bending torque on the femur during walking (Dallmann *et al* 2016). Therefore, we developed a one-group technique with which to estimate the stimulus force required to produce the recorded afferent discharge.

The one-group technique estimates the stimulus force as follows. First, a forward model (i.e. force in, discharge out) is tuned to reproduce the discharge in response to one stimulus from one experimental recording. The forward model is now a model of that particular CS group (e.g. cockroach proximal tibia CS). Second, the output of the corresponding inverse model (i.e. discharge in, force out) is calculated in an iterative way. For each 'time step' of the discharge pattern, the algorithm uses Brent's method to calculate what stimulus force (i.e. the inverse model's output) would be required for the forward model's response to match the provided discharge pattern (i.e. the inverse model's input). Because CS discharge is so dynamic, multiple values of stimulus force may cause the same discharge pattern. Therefore, once the forward model's response matches the discharge pattern, an algorithm searches for the largest and smallest forces that could still produce a match (this algorithm is akin to a line-search (Dennis and Schnabel 1983) and is described in the supplementary materials). When the discharge (i.e. the inverse model's input) is greater than 0, there is usually no difference between the largest and smallest forces it calculates. However, because CS discharges are minimal or silent when forces decrease, there may be a wide range of forces that would produce no discharge or sharp decreases in discharge frequency. When this occurs, the envelope between the largest and smallest forces 'opens' and the inverted model's accuracy decreases. Results from the one-group technique are shown in figures 9 and 10.

2.7. Model inversion: two-group technique

To improve the accuracy of the inverse model while the discharge of one CS group decreases or ceases, a two-group technique that uses simultaneous

recordings from antagonistic CS groups was developed. In our experiments, we used recordings from stick insect tibial CS groups 6A and 6B. Conceptually, the two-group technique is identical to the one-group technique except in two ways. First, the two-group technique maintains two separate CS forward models (i.e. force in, discharge out), one for each group, where both forward models receive the same force stimulus, except that the sign of one group's stimulus is inverted (i.e. made negative) to reflect the sensitivity of groups 6A and 6B to forces in opposite directions (Zill *et al* 2011). Second, the two-group technique tries to calculate one force stimulus that would simultaneously equate the sensory discharge of both forward models to its corresponding experimental recording at each time step; if this cannot be accomplished at a particular time step, the algorithm minimizes the sum of the square of the deviation between each model's sensory discharge and its corresponding recording. In this way, the inverse model calculates one output, the stimulus force, based on two inputs, the sensory discharge of group 6A and 6B. Results from the two-group technique are shown in figure 11.

2.8. Model simulation

All modeling was conducted in Matlab 2020b (The Mathworks, Natick, MA). Model dynamics were simulated with the ode15s function. Gradient-based optimization was conducted with the fmincon function. All other code, including the GA and one- and two-group techniques for inverting the model were written for this project. https://github.com/nss36/campaniformSensillaModeling

3. Results

3.1. Model responses to simple force stimuli

To test if the model can reproduce the documented responses to simple force stimuli, we first tuned parameter values to reproduce CS response to a single ramp-and-hold (RAH) force stimulus. The parameter values found are displayed in table 2. The stimulus, the response of the cockroach proximal tibial sensilla to the stimulus, and the model's response are shown in figure 3(a). The responses of both the CS and the model show a sharp initial increase (0%–5% stimulus), followed by a decrease in its slope (5%–15% stimulus), followed by a dramatic adaptation (15%–80% stimulus), and finished by total silencing (80%–100% stimulus). This response is typical for CS groups across the legs of multiple insect species (Zill *et al* 2018).

Without altering the parameter values, the model reproduced the responses to multiple additional stimuli. Figure 3(b) shows that the model reproduced the CS response to a 'naturalistic stimulus', i.e. a joint torque experienced during walking that lacks a static hold phase (Dallmann *et al* 2016). Similar to results reported in cockroach CS, the model's response to the naturalistic stimulus varied greatly from its response to the RAH stimulus. In particular, the naturalistic response rose less quickly, peaked lower, and adapted less rapidly than its response to the RAH stimulus (figure 3(c), see also figure 9(c) of (Zill *et al* 2018)). Furthermore, the model reproduced the responses to additional RAH stimuli (figure 3(d)). In particular, as the speed of force application increased (i.e. $\frac{du}{dt}$ of the RAH stimulus), the model's responses scaled as observed in animal recordings. These results suggest that the model captures the underlying dynamics of load sensing in insect legs.

To evaluate whether our model performs as well as a fractional derivative model, figure 3(a) also includes the fractional derivative of the input force ($a = 40.6, b = 0.631$ in equation (19)). Both models mimic the discharge pattern with a small mean absolute error (MAE) of about 5 AP/s (table 3). Similar accuracy may be expected because this trial was used to tune the parameter values. However, when comparing the model responses in figure 3(b), which the models were not tuned to reproduce, the fractional derivative model's average error is more than 50% greater.

To test if the model encodes force stimulus u and its rate of change $\frac{du}{dt}$ as documented in the animal, we subjected the model to a number of RAH stimuli of varying amplitudes, rates, and offsets. The model responses in figure 4(a) and the summary in figure 4(b) show that the model reproduced the result from Ridgel *et al* (Ridgel *et al* 2000). In the animal, the proportionality constant of this logarithmic relationship (i.e. k in figure 4) spans 0.28 to 0.57 given a list of stimulus amplitudes; in testing our model with the same amplitudes, we found proportionality constants spanning a similar range, 0.27 to 0.46.

Furthermore, it has been observed that the encoding of $\frac{du}{dt}$ is less sensitive to the application of tonic forces, as indicated by the narrower range of proportionality constants as the stimulus is offset (Ridgel *et al* 2000). The responses in figure 4(c) and the summary in figure 4(d) show that the model mimics this result as well. In the animal, the proportionality constant of this logarithmic relationship, k, spans 0.34 to 0.43 given a list of stimulus offsets; in testing our model with the same offsets, we found proportionality constants spanning a similar range, 0.25 to 0.38. The change in proportionality constants was lower than that in response to changing the amplitude in both the animal and the model, suggesting that they are both less sensitive to offsets than to stimulus amplitudes. In both figures 4(b) and (d), the model's discharge encoded the rate of change of the stimulus with similar proportionality as in the animal, despite not having been tuned to do so.

Figure 5 shows that the analytically calculated responses agree with the simulated responses. Because

Table 3. Summary of nonlinear model's accuracy compared to the fractional derivative model's accuracy. All values are MAE, measured in action potentials per second (AP/s). The first column indicates the trial in question. The second column includes the MAE between the nonlinear model presented in this paper and the experimental recordings. The third column indicates the MAE between the traditional fractional derivative model and the experimental recordings. The final column indicates the difference in fit between the two models, with positive values indicating that the nonlinear model fits the data better than the fractional derivative model. Negative values (i.e. where the fractional derivative model performed best) are written in red for emphasis.

Figures	Mean abs. err. nonlinear (AP/s)	Mean abs. err. fractional (AP/s)	Nonlinear improvement (AP/s)
Figure 3(a)	4.85	5.56	0.71
Figure 3(b)	9.87	16.22	6.35
Figure 7(a), 6A	6.49	6.11	**−0.38**
Figure 7(a), 6B	47.3	69.8	22.5
Figure 7(b), 6A	5.58	5.59	0.01
Figure 7(b), 6B	65.0	60.3	**−4.70**
Figure 7(c), 6A, left	6.26	5.59	**−0.67**
Figure 7(c), 6A, center	3.90	4.65	5.61
Figure 7(c), 6A, right	2.25	7.86	3.25
Figure 7(c), 6B, left	55.6	54.8	**−0.78**
Figure 7(c), 6B, center	60.8	54.6	**−6.15**
Figure 7(c), 6B, right	17.5	24.1	6.64
Figure 7(d), 6A, left	2.50	5.75	3.25
Figure 7(d), 6A, center	2.02	8.89	6.88
Figure 7(d), 6A, right	2.33	6.56	4.23
Figure 7(d), 6B, left	24.7	36.9	12.2
Figure 7(d), 6B, center	20.2	27.9	7.70
Figure 7(d), 6B, right	14.5	21.1	6.60

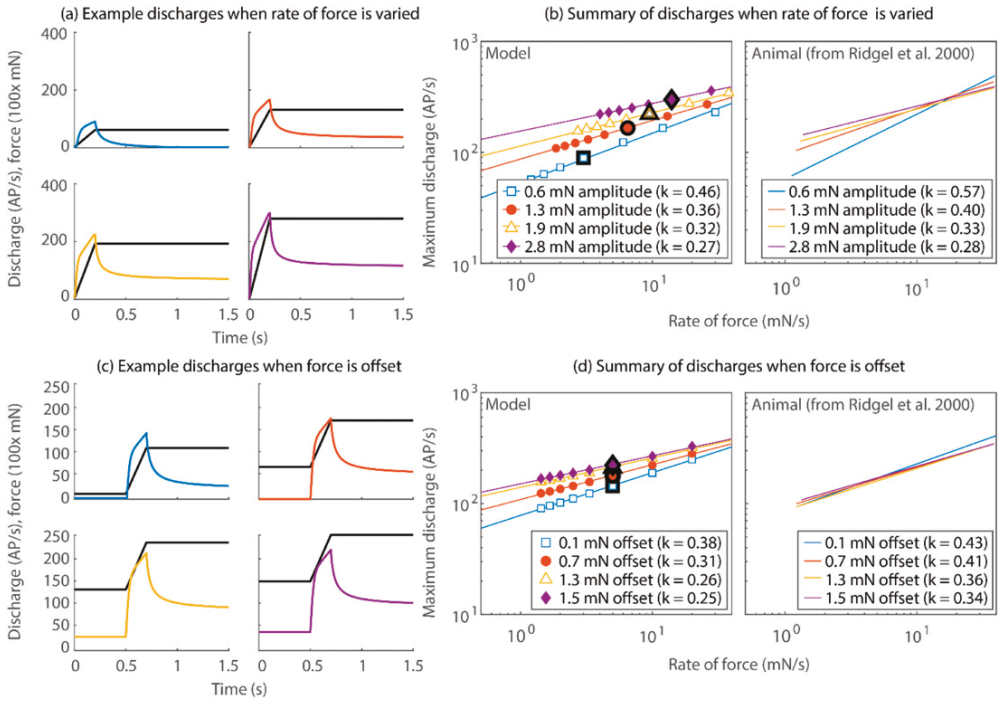

Figure 4. The model replicated rate-encoding properties of CS sensory discharge. In each part of this figure, many trials were simulated to characterize gross response properties. The plots in the left column show representative raw simulation results, and the plots in the right column summarize the results of many simulations and experimental results alongside results from (Ridgel *et al* 2000). Points in the summary plots that correspond to the example responses are outlined in black. (a) Example model responses to stimuli with varying rates of force (i.e. constant amplitude, varying ramp duration). (b) The peak discharge during a ramp-and-hold stimulus reflected the rate of change of the stimulus (i.e. ramp slope). Reprinted by permission from Springer Nature Customer Service Centre GmbH: Springer Nature, Journal of Comparative Physiology A [Ridgel *et al.*] (c) 2000. The greater the stimulus amplitude, the higher the peak discharge, and the less sensitive the discharge was to the stimulus rate of change (i.e. line of best fit has a slope, k, closer to 0). (c) Example model responses to stimuli with varying tonic offsets. (d) The peak discharge during a ramp-and-hold stimulus was affected by constant offset forces (note varying values of k). The model was less sensitive to offsets (i.e. narrower range of values of k) than to the amplitude of the stimulus, as observed in cockroach tibial CS (Ridgel *et al* 2000). Reprinted by permission from Springer Nature Customer Service Centre GmbH: Springer Nature, Journal of Comparative Physiology A [Ridgel *et al.*] (c) 2000.

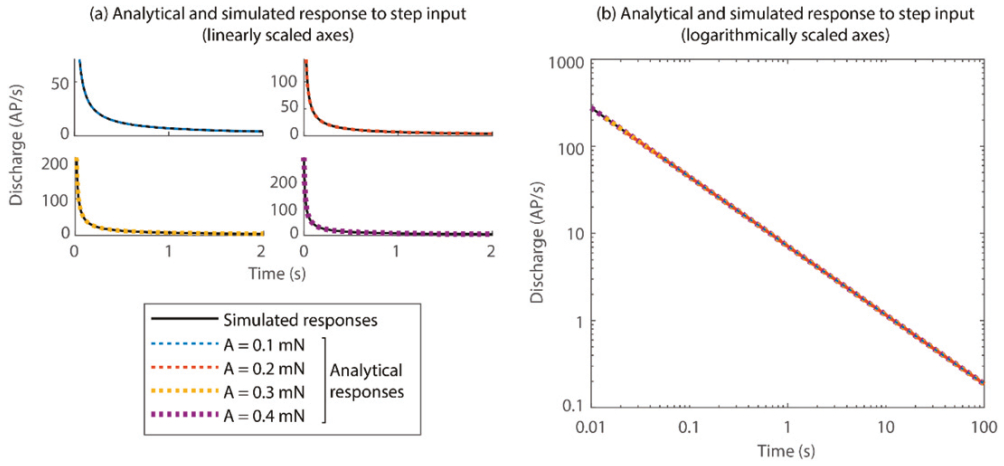

Figure 5. The model's adaptation after a step input follows a power-law function, as observed in discharge recordings from cockroaches (figure 1(c) and (Ridgel *et al* 2000)). (a) The model's responses to step inputs of varying amplitudes were plotted over time. Simulated responses are plotted in solid black lines, and the exact analytical responses are plotted in dashed lines whose colors indicate the stimulus amplitude. (b) The same 4 responses shown in (a), plotted on logarithmic axes. The responses fall along a straight line, indicating that they decay according to a power-law, as opposed to exponential decay.

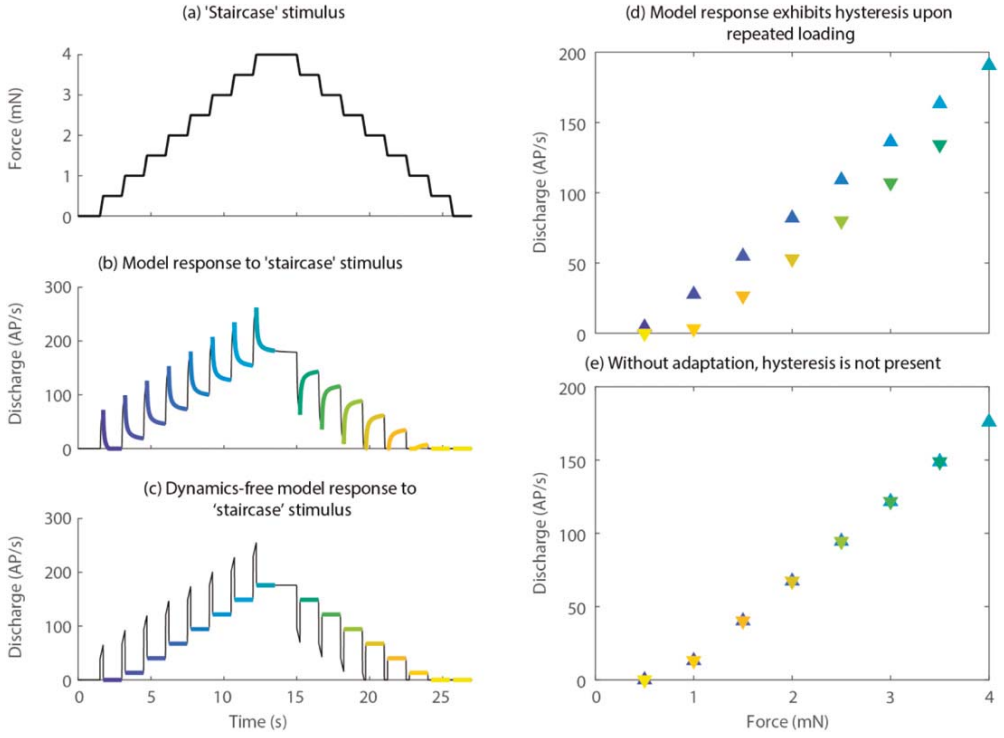

Figure 6. As observed in insect CS, the model response exhibited hysteresis under cyclic loading. (a) To test the model response, a 'staircase' stimulus force was generated, in which the stimulus repeatedly 'rose' to a new level, and then 'ran' at a constant level for a portion of time (e.g. (Ridgel *et al* 2000)). (b) The full dynamic model adapted over time in response to each new force level. The response during each run period, during which the force is static, is shaded on a blue-to-yellow continuum over time. (c) Reformulating the model to explicitly rely on the rate of change of the stimulus produced a cosmetically similar response to the staircase stimulus. However, the signal did not adapt to the new force level during the run portion of the stimulus. (d) Plotting the model's average response during the run portion of the stimulus reveals that the response was different depending on whether the model was loaded or unloaded to that level. (e) Plotting the dynamics-free model's average response during the run portion of the stimulus shows that no hysteresis was present. This difference between the model formulations' responses shows that hysteresis may simply be a consequence of the adaptive response that gives rise to CS's sensitivity to force rate of change. Reprinted by permission from Springer Nature Customer Service Centre GmbH: Springer Nature, Conference on Biomimetic and Biohybrid Systems [Szczecinski *et al.*] (c) 2020.

the model is nonlinear, it is not guaranteed that an analytical solution can be found (Boyce and DiPrima 1967). All plots in figure 5 show that the analytical response from equation (11) lies over the simulated

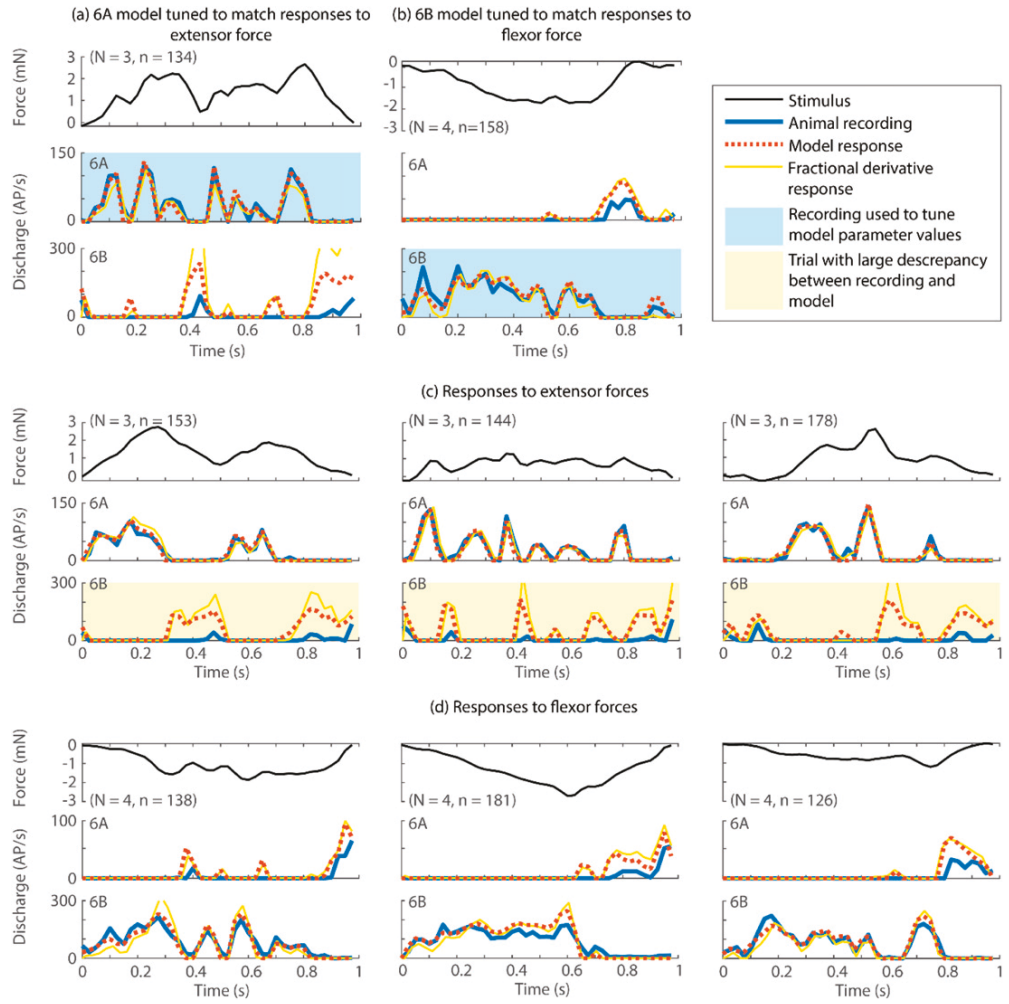

Figure 7. The model reproduced the animal recordings of CS afferent discharge in response to joint torques recorded from freely walking insects (Dallmann *et al* 2016). The model was tuned two different ways to replicate the unique response characteristics of group 6A and 6B tibial CS. The key in the upper-right corner of the figure applies to all plots. (a) A model of group 6A was produced by tuning the model's parameters to minimize the mean squared error between its response and the response of group 6A, which primarily responds to torques imposed by extensor contraction (plot shaded in blue). (b) Separately, a model of group 6B was produced by tuning the model's parameters to minimize the mean squared error between its response and the response of group 6B, which primarily responds to torques imposed by flexor contraction (plot shaded in blue). (c) Without retuning, the group 6A model reproduced the discharge in response to extensor torques from individual steps. (d) Without retuning, the groups 6A and 6B models reproduced the discharge in response flexor torques from individual steps.

responses. The supplementary materials show that this agreement is within the tolerances of the numerical integration algorithm (figure S1). Thus, the model has an exact analytical solution in response to a step input, and the solution is power-law decay over time, a hallmark feature of CS responses.

Figure 5 also shows that the model's output adapts to tonic force as a power-law function of time, one of the key features of CS responses. The plots in figure 5(a) show how the response adapted to a step stimulus when the axes are linear. Characteristic of power-law adaptation, the adaptation appears to 'stall' almost immediately after stimulus onset, decaying at an ever-slowing rate. Power-law responses appear as straight lines when the time and discharge axes are scaled logarithmically. Figure 5(b) plots the responses from (a) on the same set of logarithmically scaled axes for direct comparison. All the responses follow a straight line, indicating power-law decay.

CS discharge exhibits hysteresis, in which the average response over time to a particular load amplitude is different depending on whether the force increased or decreased to that amplitude. Hysteresis is quantified by loading the CS with a 'staircase' function, in which the force is increased in steps and then decreased in steps (figure 6(a)). Due to hysteresis in load encoding, the average discharge due to any single force level will be higher on the way 'up' the staircase than on the way 'down', i.e. it will depend on both the instantaneous force and its history (Ridgel *et al* 2000).

The model replicated this effect, with the transient response biasing the mean discharge upward during increasing steps and downward during decreasing steps (figure 6(b)), despite the model

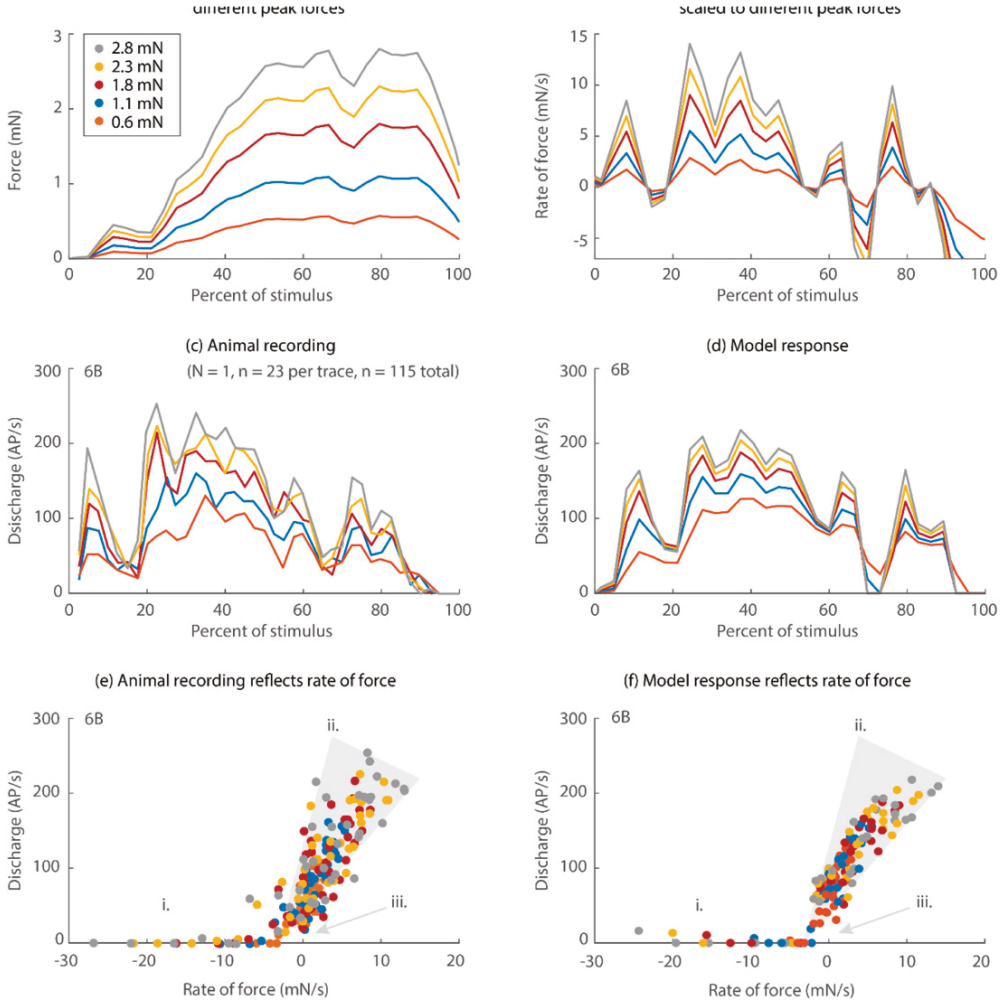

Figure 8. The model mimicked animal recordings of group 6B CS subjected to dynamic force stimuli scaled to different magnitudes. (a) The single-step stimulus from figure 7(b), scaled to different levels: 0.6, 1.1, 1.8, 2.3, and 2.8 mN. (b) Scaling the magnitude also scales the rate of change of the stimulus. (c) In animal recordings, the level of fluctuation in the animal responses tended to increase with the scaling factor of the force. (d) Model responses formed a similar spectrum in response to scaled forces. This includes responses that reflect the rate of change of the stimulus and responses that 'bunch' together at some points. (e) Animal recordings encoded the rate of change of force and exhibited three identifiable features: (i) generally no activity during negative rates of change of force; (ii) activity that generally encoded the positive rate of change of force; and (iii) activity in response to small decreases in force, provided that the magnitude of the force was large. (f) Model responses correlated to changes in force in the same ways as the animal recordings.

being formulated to have exactly one equilibrium point. The model's response to both step-up and step-down stimuli will approach the same value as time goes to infinity. However, due to the power-law decay, the response approaches the equilibrium more slowly as time progresses, meaning that in a practical sense, the CS and model exhibit hysteresis. When subsequent steps were considered, the responses form a 'hysteresis loop' (figure 6(d)), which is generally considered undesirable for engineered sensory systems.

Despite hysteresis being undesirable for engineered sensors, we hypothesize that hysteresis and rate-sensitivity are mechanistically linked. Recall from the methods that the adaptation in our model gives rise to the rate-sensitivity of the response. If this adaptive response were removed, the model would no longer encode $\frac{du}{dt}$. However, it was possible to reformulate the model in a simpler way that abandoned adaptation to encode the rate of force directly:

$$y = \max(a\dot{u}^b + cu + d).$$

This simplified model's discharge directly encodes $\frac{du}{dt}$, and so must encode force amplitude and rate in a similar way as the full model. However, this model's response (figure 6(c)) showed no apparent adaptation or hysteresis in response to the staircase stimulus. Generating a plot as in figure 6(d) reveals that no hysteresis occurs without the adaptation (figure 6(e)). This suggests that the rate-sensitivity, adaptive responses, and hysteresis observed in insect CS are all interdependent characteristics that may stem from the same underlying mechanism.

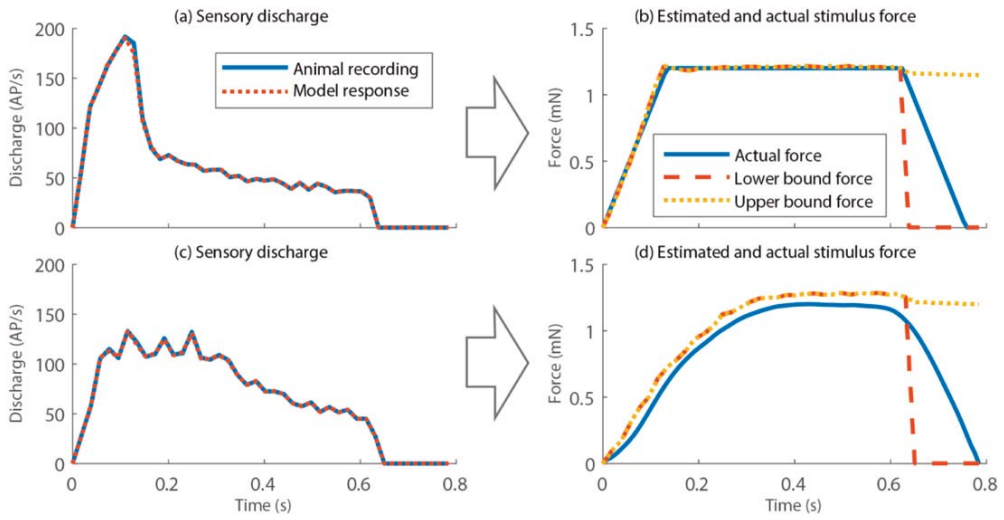

Figure 9. Using the one-group model inversion technique, the model could recreate features of the force waveform applied to the tibia based on the sensory discharge recording. (a) The model inversion process used the comparison between the animal recording and model response to predict the force. (b) The inverted model accurately estimated the slope of the stimulus as well as the amplitude of the hold phase. This was unsurprising because this trial was used to tune the model parameters. However, this trial showed that since CS are strongly inhibited by decreasing forces, the one-group inversion technique failed to estimate them, even when recreating the data used to tune the model. (c) The model inversion technique could follow the sensory discharge exactly for this stimulus. (d) The model inversion technique performed similarly as in (b) when provided the discharge pattern from a more dynamic stimulus. The model estimated the rate and amplitude of the non-decreasing portion of the force stimulus, but again failed when the force began to decrease rapidly.

3.2. Model responses to walking force stimuli

To better validate that the model captures the dynamics of CS discharge, we subjected the model to highly dynamic 'naturalistic stimuli', i.e. the torque experienced by the leg as a stick insect walks on a level surface (Dallmann *et al* 2016). Figure 7 shows the eight naturalistic stimuli used, the corresponding response of stick insect groups 6A and 6B tibial CS, and the response of the model. Group 6A and group 6B encode force complementarily: group 6A to forces and rates of force (i.e. dF/dt) imposed by extensor contraction resisted by external tibia flexion, while group 6B responds to forces and rates of force imposed by flexor contraction resisted by external tibia extension (Zill *et al* 2011). Thus, two instances of the model were tuned: a group 6A instance and a group 6B instance. The 6A instance received the force stimulus as indicated throughout figure 6 and was tuned using only one trial (figure 7(a)). The 6B version received an identical but negative force stimulus due to its orientation relative to group 6A (Zill *et al* 2011) and was tuned using only one, separate trial (figure 7(b)). Making the force negative also changes the sign of dF/dt, meaning that both groups 6A and 6B may respond to the same force stimulus, even if the force itself is biased in one direction or the other. The parameter values for each instance of the model (i.e. 6A and 6B) are listed in table 2.

The same parameter values enabled the model to reproduce group 6A discharges to all eight stimuli tested. Predicted discharges appear most accurate in response to extensor torques, group 6A's preferred direction (figure 7(c)). The group 6B model tuning captured the dynamics of flexor torques most accurately (figure 7(d)). Less accurate responses (figure 7, highlighted in yellow) occurred to force decreases, which in the animal, were often delayed in time and firing accelerated as forces approached zero. These discharges apparently result from cuticle properties (viscosity) that will, in future work be incorporated into the model (see discussion).

The model's ability to capture the dynamics of CS discharge was further validated by the way in which its responses varied as the dynamic force stimulus was scaled. Figure 8(a) shows the naturalistic stimulus from figure 7(b), scaled to five different levels. The stimuli's rates of change are shown in figure 8(b). The responses of the animal's group 6B CS to the scaled stimuli are shown in figure 8(c). These responses appear to correspond more strongly to the rate of change of the force than to its amplitude, exhibiting steep decreases in firing frequency in response to intermittently decreasing forces around 10% and 70% of the stimulus duration. The model responses mimicked these features, with a similar 'bunching' of the traces occurring around 10% and 70% of the stimulus duration (figure 8(d)). However, because the model is deterministic but animal discharge is stochastic, the animal responses to differently scaled forces sometimes 'cross' one another in a way that the model responses do not.

Plotting the group 6B discharge versus the rate of change of the force shows that the discharge strongly reflected the rate of change of force, despite how

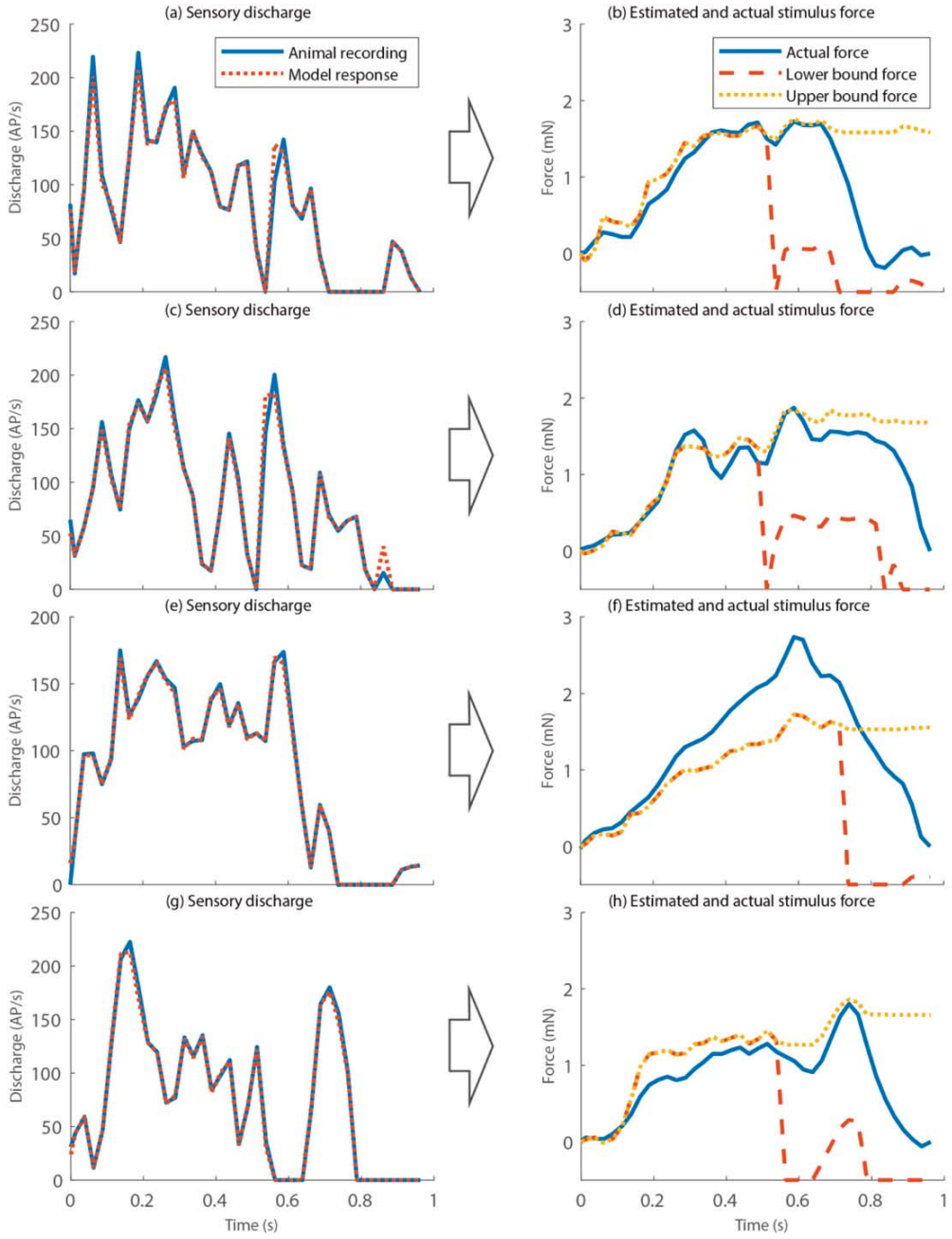

Figure 10. Using the one-group model inversion technique, the model could recreate some of the force stimuli used in figures 7(b) and (d) based on the sensory discharge recording of the group 6B CS alone. In each case, the model minimized the difference between the animal recording and model response ((a), (c), (e) and (g)) to predict the applied force, as long as the discharge did not reach 0 AP/s. At one time in each trial ($t = 0.5$ in (b); $t = 0.5$ in (d); $t = 0.7$ in (f); $t = 0.55$ in (g)), the discharge reached 0 AP/s, causing the envelope between the lower and upper force bounds to open very widely, limiting the utility of the analysis. Interestingly, the lower bound force continued to respond to rapid increases in the force after the envelope opens ($t = 0.55$ in (b); $t = 0.55$ in (d); $t = 0.9$ in (f); $t = 0.65$ in (h)).

dynamic the stimulus was and how adaptive the response was (figure 8(e)). Three main features are observed in the animal recordings. First, when the rate of force was very negative (i.e. less than 5 mN s^{-1}), the discharge was always 0 AP/s or very nearly 0 AP/s (figure 8(e), (i)). This is because decreasing forces, no matter their amplitude, tended to silence CS discharge. Second, discharge was roughly proportional to positive rate of force (figure 8(e), (ii)). Finally, discharge did occur in response to forces that decrease slowly, potentially due to tonic sensitivity, as well as latencies in afferent responses and conduction speed of APs (figure 8(e), (iii)). The model inherently reproduced all three of these response features, albeit with less variability than observed in the animal (figure 8(f)).

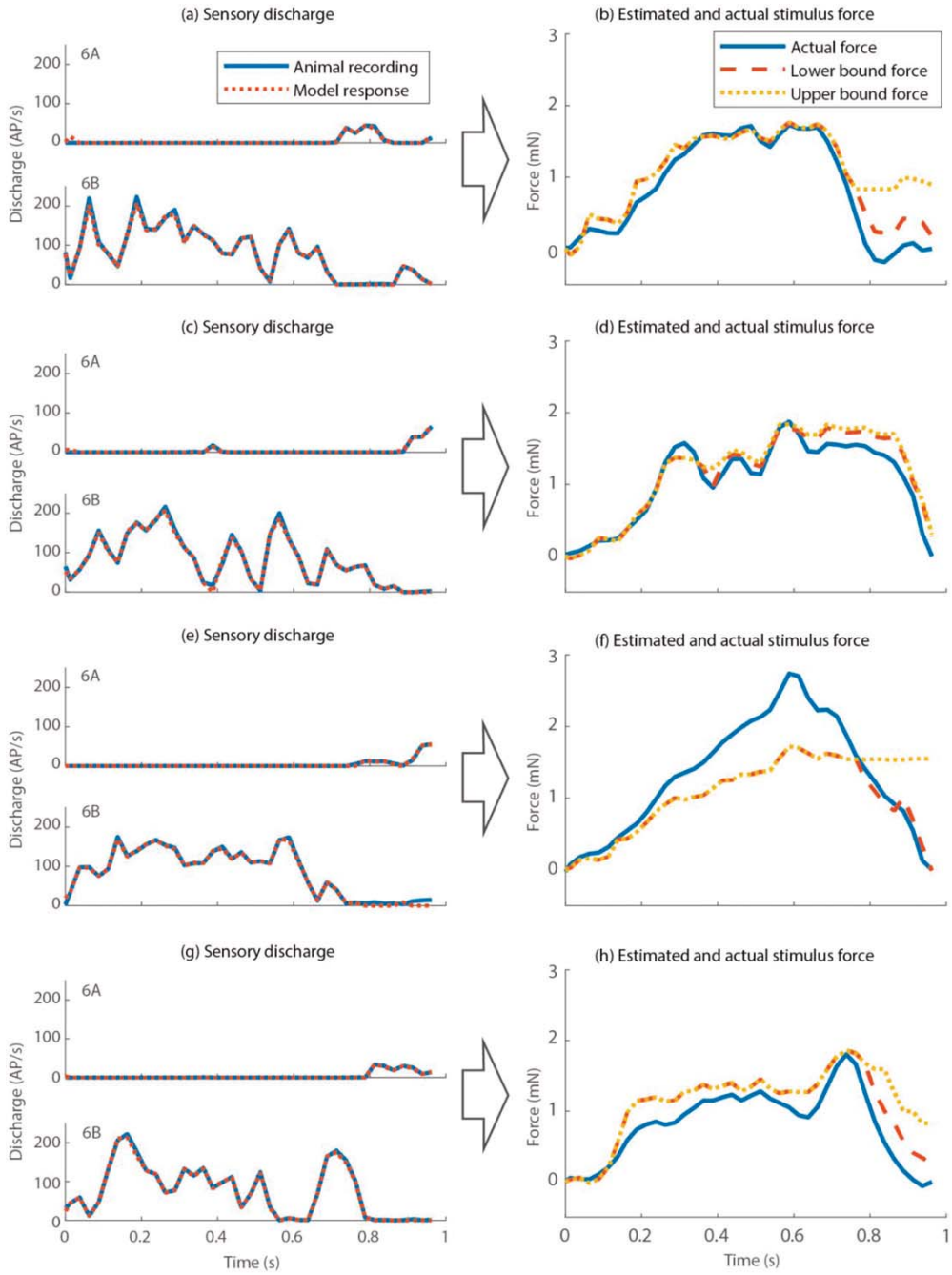

Figure 11. The two-group model inversion method more accurately estimated decreasing forces than the one-group inversion method. The inverted model could approximate the stimulus forces used in figures 7(b) and (d) based on the groups 6A and 6B CS recordings. Considering the activity of both groups 6A and 6B ((a), (c), (e) and (g)) decreased the range of the estimated force relative to the trials in figure 10, i.e. the lower and upper force bounds overlap at every point ((b), (d), (f) and (h), respectively). At points where the match was poor (e.g. $t = 0.6$ s in (f)), the estimated force still mimicked the fluctuations in the force stimulus.

3.3. Inverting the model to estimate force stimuli from CS discharge recordings

The model can be 'inverted', in which sensory discharge recordings are provided as inputs, and the model computes what force would be necessary to produce the recordings. This functionality could enable experimentalists to estimate the forces acting on the legs based on CS recordings from standing or walking animals (Noah *et al* 2001, 2004, Ridgel *et al* 2001, Keller *et al* 2007). Although previous studies of other strain-sensitive organs, e.g. spider lyriform organs, suggest that forces from muscle co-contraction acting on the cuticle may complicate such a method (Blickhan and Barth 1985, Blickhan *et al* 2021), our analysis suggests that due to the placement of insect muscle attachments and CS on the tibia, muscle co-contraction should not affect CS discharge (see figure S2 in the supplementary

materials). The one-group and two-group techniques for this inverted model are described in the methods.

Figure 9 shows the results of inverting the model using recordings from only one CS group. Because these recordings were from the proximal tibial CS of the cockroach (figure 9(a)), the model parameter values from the first column of table 2 were used. Figure 9(b) shows that the inverted model could accurately estimate the stimulus force that produced the discharge pattern while the stimulus force was increasing or held constant. This is because discharge depends both on the level of force stimulus and its positive rate of change. Because the model output cannot become negative in response to decreasing or negative forces, it cannot predict the amplitude of the force once the discharge pattern goes to 0. However, our method did 'envelop' the force by computing a lower and upper bound of possible force. The model correctly detected that the force must have decreased when $t \approx 0.65$ s in order to silence the discharge. Many rates of decrease could have driven the discharge to 0, bounded by the small decrease in the yellow trace and the large decrease in the red trace. The true force stimulus was contained between these bounds. Figures 9(c) and (d) show that a similar result was produced when the response from the naturalistic stimulus from figure 3(b) was input. The inverted model accurately estimated the force stimulus while the force was increasing or constant but broke down once the force began decreasing rapidly. As in figure 9(b), the estimated force in figure 9(d) was bounded during the decrease.

To further validate the performance of the inverted model, we used the group 6B model (parameters in rightmost column of table 2) to predict the stimulus force that generated the discharge patterns from figures 7(b) and (d). These discharge and force patterns are highly dynamic and served as a thorough test of our model's capabilities. Figure 10 shows that the inversion technique performed comparably well as in figure 9. However, because the discharge patterns in figure 10 intermittently went to 0, the force envelope opened drastically about halfway through each trial, limiting the accuracy and utility of the inverted model. To prevent the force envelope from opening, we developed the two-group technique, which simultaneously considers group 6A discharge to extract information about the rate and amplitude of force decreases (see methods).

Figure 11 shows that the two-group technique improved the performance of the inverted model. The force envelope always remained much more closed than in the one-group technique, with the lower and upper bounds often equal. One noticeable exception was the end of the third trial, in which the lower bound traced the force accurately, but the upper bound remained relatively high. This may be because both groups were nearly silent during this period, giving the model limited information from which to estimate the force. In general, incorporating recordings from both groups 6A and 6B gave the model information about how quickly force was changing in both directions (i.e. increasing and decreasing), producing more accurate tracking of the stimulus force over time.

4. Discussion

This study described and analyzed a simple nonlinear dynamical phenomenological model of how sensory afferents from groups of CS on the legs of insects encode force. The model is simple because it includes only one input, the stimulus force; one dynamical adaptive variable; and one output, the difference between the stimulus and adaptive variable, plus some additional terms. The model is nonlinear and dynamical because the adaptive variable changes according to a nonlinear function, which we predicted and then tuned based on empirical data. Finally, the model is phenomenological because it reproduces the input-output relationship between the stimulus force applied to the leg and the firing frequency of the afferent nerve without any explicit reference to the mechanics or nervous system of the animal. Despite its simplicity and abstraction, this model predicts all dynamic response properties of leg CS reported in the literature (adaptation, rate-sensitivity, and hysteresis) to simple force stimuli and highly dynamic force stimuli. It can be inverted to predict the force stimulus required to produce recorded sensory discharge. This model reproduces CS discharges more accurately than a fractional-derivative model in most of the cases tested and may be more readily related to neural and mechanical mechanisms because of its integer-order dynamics (i.e. no fractional derivatives, (Chapman and Smith 1963, French 1984)).

In our phenomenological model, the 'adapting variable' does not refer to any specific adaptation mechanism. Such adaptation could arise from neural properties such as spiking rate adaptation in the afferents (Gerstner, 2000, French and Torkkeli 2008, Mihalas and Niebur 2009, Szczecinski *et al* 2020a, 2020b), macroscopic mechanical properties of the cuticle such as viscoelastic creep (Brown and Stein 1966, Chapman *et al* 1979, Hillerton 1984), adaptive properties of molecular transduction structures within the sense organ (Gillespie and Walker 2001), or other sources. Although it has been suggested that multiple simultaneous relaxation processes within the exoskeleton and nervous system combine to produce adaptation (Brown and Stein 1966), investigations of spider slit sensilla suggest that adaptation is dominated by neural properties rather than mechanical effects. Specifically, afferent firing adapts even in response to direct electrical stimulation (French 1984), and simulations suggest that the dynamics of a slowly inactivating Na^+ channel can produce similar sensory adaptation over time, providing a plausible mechanism by which

this adaptation arises (French and Torkkeli 2008). However, due to differences in anatomy and available experimental techniques between spiders and insects, it is uncertain if the same is true of CS. We plan to perform similar experiments in insect CS to determine if neural properties contribute to the observed adaptation.

4.1. Future applications

One motivation for this model was to endow a legged robot with CS-like load sensing. Some insect-like robots include strain gauges in some of the locations where CS appear on insect legs (Szczecinski *et al* 2015, Goldsmith *et al* 2020), and the feedback they provide coordinates the timing (Szczecinski *et al* 2017) and magnitude (Szczecinski and Quinn 2017) of motor output as observed in animals (Zill *et al* 2004, Buschmann *et al* 2015, Tuthill and Wilson 2016, Bidaye *et al* 2017). Furthermore, care is taken to dynamically scale the robot's mechanics and movement speeds to match those of an insect (Sutton *et al* 2021). Using such a robot as a neuromechanical model of an insect, the impact of CS-like load processing on the control of walking can be tested.

Although this study did not present data from a robot, in future studies we plan to implement this model as a real-time filter for feedback from strain gauges on the legs. We expect that such a filter would improve the timing control of the actuators during walking. Current biologically inspired walking controllers use load feedback from strain gauges to detect when the leg is supporting the body and subsequently alter the phasing of pattern generators in the ventral nerve cord to generate stance phase motor activity (Goldsmith *et al* 2020). To achieve proper coordination, load feedback must often be amplified to strongly inhibit parts of the network that generate the swing phase, but such amplification also amplifies electrical and vibrational noise that interferes with proper coordination. We expect that the CS model will improve network performance due to its sensitivity to increasing forces. Specifically, when the leg first makes ground contact, the CS model will initially produce strong discharge with which to inhibit swing phase motor networks and transition the network into the stance phase. As the stance phase progresses, further increases in force would reinforce the activity of stance phase motor networks. Toward the end of the stance phase, load on the leg may decrease due to the forces of other legs (Dallmann *et al* 2017) or the orientation of the leg itself (Cruse 1985), which would silence discharge of CS that encode load increases and activate CS that detect load decreases (Zill *et al* 2009), eliciting an activation (or disinhibition) of swing phase control networks.

We also expect that a strain feedback filter like the model in this study would improve the magnitude control of the actuators during walking. Many studies in invertebrates and vertebrates describe positive force feedback, in which force feedback excites agonist muscles to resist the sensed load (Prochazka *et al* 1997a, 1997b, Zill *et al* 2014, 2015). One would expect such a system to be unstable unless closely monitored by the nervous system. However, a more parsimonious explanation for the apparent stability of legged animals utilizing positive force feedback is that the CS (and Golgi Tendon Organs (Jami 1992)) encode the rate of change of force or 'yank' (Lin *et al* 2019) much more strongly than the tonic force level (Zill *et al* 2021). In this way, the feedback may regulate itself, by effectively reducing its gain as it adapts to constant loads. Applying our model to robotic and simulation studies will enable us to directly compare robot performance with different forms of force feedback and better understand how sensory dynamics may contribute to the stability of complete behaviors.

Another motivation for this model is to facilitate future experiments with animals. One possibility would be to record from the CS of freely walking insects and use this model to estimate the forces and torques experienced during locomotion. Because muscles actuate limbs by generating torque about a joint, insight into the control of locomotion can be gained by measuring the torques acting on each individual leg joint. Typically, the torque acting about each joint during locomotion is calculated by simultaneously measuring ground reaction forces (e.g. via a force plate) and leg kinematics (e.g. via a motion-tracking camera system) and building a kinematic model to approximate the torque acting about each joint (Murray *et al* 1994, Witte *et al* 2002, Dallmann *et al* 2016). Such a method is difficult to employ for some insects, for example cockroaches, whose legs are oriented under their bodies with flexed posture. Furthermore, this method is expensive, complicated, and requires much expertise and external equipment. Recording CS discharge from freely-standing insects (Noah *et al* 2001, 2004, Ridgel *et al* 2001, Keller *et al* 2007) and then using our model to estimate joint torques from the discharge pattern may provide a useful alternative method with relatively low cost and complexity.

4.2. Limitations of the model

Although the model captures the response dynamics of CS in many contexts, the model's output deviates starkly from the recorded 6B discharge in the trials plotted in figures 7(a) and (c) (shaded yellow). In many tests, the model predicts vigorous discharges to force decrements while biological responses of CS are both smaller in magnitude and often delayed in onset. The source of CS's sensitivity to force decrease is unclear. These responses appear to be dependent upon mechanical properties of the leg cuticle as the receptors do not show ON-OFF discharges in response to direct stimulation of the caps (Zill *et al*

2011). Further study of the effects of the viscoelastic properties of the exoskeleton in response to force decreases may clarify the source of apparent dampening of afferent discharges and further improve the accuracy of the model. The results of such study could be used to extend the model, e.g. by explicitly modeling viscoelastic leg dynamics in addition to other dynamic processes that cause afferent firing rate adaptation.

The recordings themselves may also contribute to the disagreement between the model and animal data. Ordinarily, discharges can be classified as small and large amplitude on extracellular recordings (Zill *et al* 2011). However, when afferents discharge rigorously, e.g. at the onset of a stimulus, multiple APs from differently-sized caps may coincide, limiting the accuracy of measurement of afferent firing frequency. Because the model so accurately mimics responses in all other contexts tested, it is possible that action potential superposition led to inaccurate determination of the 6B firing frequency, meaning that the model's output reflects the actual afferent discharge frequency. However, further work is needed because both our model and the fractional derivative model predicted robust afferent firing during force decreases when none (or very little) occurred in the animal (cf figures 7(a) and (c)).

4.3. How dynamic load feedback may enhance legged locomotion

This study models the dynamics of CS afferent discharge and shows how adaptation to tonic forces and rate-sensitivity may be mechanistically related. Processing load feedback this way should have implications for the control of locomotion. There is a growing call in motor control to focus on the rate of change of force, or 'yank', in various animal systems (Zill *et al* 2018, 2021, Lin *et al* 2019), particularly since multiple load sensing organs across phyla appear more sensitive to yank than force (spider slit sensilla, (Torkkeli and French 2002); vertebrate Golgi tendon organs, (Jami 1992); insect CS, (Zill *et al* 2018)). Measuring yank rather than the instantaneous force level may enable the nervous system to make predictions about the future state of the load, for example, by linearly extrapolating the force into the future, e.g. $u(t+\Delta t) \approx u(t) + \Delta t \cdot \frac{du}{dt}$. Such information may facilitate preemptive motor reactions to changing conditions, for example, initiating a leg's swing phase motor program while force is decreasing but before it disappears (Akay *et al* 2001, 2004). Such a prediction could enhance interleg coordination as neighboring legs enter the stance phase (Dallmann *et al* 2017), enable the leg to assume a new posture if the foot slips (Zill *et al* 1992), or detect postural instability before the animal falls over. However, for the nervous system to represent the instantaneous force acting on the body, it would need to 'integrate the derivative' of load over time, which would likely be prone to drift and stochasticity. Future studies could search for what neural systems are required to integrate yank over time accurately. Furthermore, modeling and robotics studies may test whether successful motor control should require integrating yank over time at all.

Acknowledgments

The authors thank Till Bockemuehl and Gesa Dinges for their thoughtful critiques and suggestions. NSF Grant 2015317 to RDQ and NSS, NSF Grant 1704436 to RDQ, DFG Research Fellowship DA 2322/1-1 to CJD.

Data availability statement

The data that support the findings of this study will be openly available following an embargo at the following URL/DOI: https://github.com/nss36/campaniformSensillaModeling

ORCID iDs

Nicholas S Szczecinski https://orcid.org/0000-0002-6453-6475
Chris J Dallmann https://orcid.org/0000-0002-4944-920X

References

Ache J M and Dürr V 2015 A computational model of a descending mechanosensory pathway involved in active tactile sensing *PLoS Comput. Biol.* **11** e1004263

Agrawal S, Grimaldi D and Fox J L 2017 Haltere morphology and campaniform sensilla arrangement across diptera *Arthropod Struct. Dev.* **46** 215–29

Akay T, Bässler U, Gerharz P and Büschges A 2001 The role of sensory signals from the insect coxa-trochanteral joint in controlling motor activity of the femur-tibia joint *J. Neurophysiol.* **85** 594–604

Akay T, Haehn S, Schmitz J and Büschges A 2004 Signals from load sensors underlie interjoint coordination during stepping movements of the stick insect leg *J. Neurophysiol.* **92** 42–51

Bidaye S S, Bockemühl T and Büschges A 2017 Six-legged walking in insects: how CPGs, peripheral feedback, and descending signals generate coordinated and adaptive motor rhythms *J. Neurophysiol.* **119** 459–75

Blickhan R and Barth F G 1985 Strains in the exoskeleton of spiders *J. Comp. Physiol.* **157** 115–47

Blickhan R, Weihmann T and Barth F G 2021 Measuring strain in the exoskeleton of spiders-virtues and caveats *J. Comp. Physiol.* A **207** 191–204

Blum K P, Campbell K S, Horslen B C, Nardelli P, Housley S N, Cope T C and Ting L H 2020 Diverse and complex muscle spindle afferent firing properties emerge from multiscale muscle mechanics *eLife* **9** 1–32

Boyce W E and DiPrima R C 1967 *Elementary Differential Equations and Boundary Value Problems* 4th edn (New York: Wiley)

Brown M C and Stein R B 1966 Quantitative studies on the slowly adapting stretch receptor of the crayfish *Kybernetik* **3** 175–85

Buschmann T, Ewald A, von Twickel A and Büschges A 2015 Controlling legs for locomotion—insights from robotics and neurobiology *Bioinspiration Biomimetics* **10** 041001

Chapman K M, Duckrow R B and Moran D T 1973 Form and role of deformation in excitation of an insect mechanoreceptor *Nature* **244** 453–4

Chapman K M, Mosinger J L and Duckrow R B 1979 The role of distributed viscoelastic coupling in sensory adaptation in an insect mechanoreceptor *J. Comp. Physiol.* **131** 1–12

Chapman K M and Smith R S 1963 A linear transfer function underlying impulse frequency modulation in a cockroach mechanoreceptor *Nature* **197** 699–700

Chung B, Bacqué-Cazenave J, Cofer D W, Cattaert D and Edwards D H 2015 The effect of sensory feedback on crayfish posture and locomotion: I. Experimental analysis of closing the loop *J. Neurophysiol.* **113** 1763–71

Cruse H 1985 Which parameters control the leg movement of a walking insect? II: the start of the swing phase *J. Exp. Biol.* 357–62

Dallmann C J, Dürr V and Schmitz J 2016 Joint torques in a freely walking insect reveal distinct functions of leg joints in propulsion and posture control *Proc. R. Soc. B.* **283** 20151708

Dallmann C J, Hoinville T, Dürr V and Schmitz J 2017 A load-based mechanism for inter-leg coordination in insects *Proc. Biol. Sci.* **284** 20171755

Dallmann C J, Karashchuk P, Brunton B W and Tuthill J C 2021 A leg to stand on: computational models of proprioception *Curr. Opin. Physiol.* **22** 100426

De Jong K A 1975 *An Analysis of the Behavior of a Class of Genetic Adaptive Systems* (Ann Arbor, MI: University of Michigan)

Dennis J E and Schnabel R B 1983 *Numerical Methods for Unconstrained Optimization and Nonlinear Equations* 1st edn (Englewood Cliffs, NJ: Prentice-Hall)

Di Paola M, Pinnola F P and Zingales M 2013 Fractional differential equations and related exact mechanical models *Comput. Math. Appl.* **66** 608–20

Dickerson B H, Fox J L and Sponberg S 2021 Functional diversity from generic encoding in insect campaniform sensilla *Curr. Opin. Physiol.* **19** 194–203

Duysens J, Clarac F and Cruse H 2000 Load-regulating mechanisms in gait and posture: comparative aspects *Physiol. Rev.* **80** 83–133

Elzinga M J, Dickson W B and Dickinson M H 2012 The influence of sensory delay on the yaw dynamics of a flapping insect *J. R. Soc. Interface* **9** 1685–96

French A S 1984 Dynamic properties of the action potential encoder in an insect mechanosensory neuron *Biophys. J.* **46** 285–9

French A S and Torkkeli P H 2008 The power law of sensory adaptation: simulation by a model of excitability in spider mechanoreceptor neurons *Ann. Biomed. Eng.* **36** 153–61

Gerstner W 2000 Population dynamics of spiking neurons: fast transients, asynchronous states, and locking *Neural Comput.* **12** 43–89

Gillespie P G and Walker R G 2001 Molecular basis of mechanosensory transduction *Nature* **413** 194–202

Goldsmith C, Szczecinski N S and Quinn R D 2020 Neurodynamic modeling of the fruit fly Drosophila melanogaster *Bioinspiration Biomimetics* **15** 065003

Harris C M, Dinges G F, Haberkorn A, Gebehart C, Büschges A and Zill S N 2020 Gradients in mechanotransduction of force and body weight in insects *Arthropod Struct. Dev.* **58** 100970

Hillerton J E 1984 Cuticle: mechanical properties *Biology of the Integument* ed ed J Bereiter-Hahn, A G Matoltsy and K Sylvia Richards (Berlin: Springer) pp 626–37

Jami L 1992 Golgi tendon organs in mammalian skeletal muscle: functional properties and central actions *Physiol. Rev.* **72** 623–66

Jonathan 2021 Fractional derivative. MATLAB central file exchange https://mathworks.com/matlabcentral/fileexchange/45982-fractional-derivative

Kaliyamoorthy S, Quinn R D and Zill S N 2005 Force sensors in hexapod locomotion *Int. J. Robot. Res.* **24** 563–74

Keller B R, Duke E R, Amer A S and Zill S N 2007 Tuning posture to body load: decreases in load produce discrete sensory signals in the legs of freely standing cockroaches *J. Comp. Physiol.* A **193** 881–91

Lin D C *et al* 2019 Yank: the time derivative of force is an important biomechanical variable in sensorimotor systems *J. Exp. Biol.* **222** jeb180414

Markin S N *et al* 2016 A Neuromechanical Model of Spinal Control of Locomotion A neuromechanical model of spinal control of locomotion *Neuromechanical Modeling of Posture and Locomotion* ed B I Prilutsky, D H Edwards (Berlin: Springer) pp 21–65

MATLAB 2020 version b (R2020b) (Natick: The MathWorks)

Mihalas S and Niebur E 2009 A generalized linear integrate-and-fire neural model produces diverse spiking behaviors *Neural Comput.* **21** 704–18

Mongeau J M, Sponberg S N, Miller J P and Full R J 2015 Sensory processing within cockroach antenna enables rapid implementation of feedback control for high-speed running maneuvers *J. Exp. Biol.* **218** 2344–54

Murray R M, Li Z and Sastry S S 1994 *A Mathematical Introduction to Robotic Manipulation* (Boca Raton, FL: CRC Press)

Naris M, Szczecinski N S and Quinn R D 2020 A neuromechanical model exploring the role of the common inhibitor motor neuron in insect locomotion *Biol. Cybern.* **114** 23–41

Noah A, Quimby L, Frazier F and Zill S 2001 Force detection in cockroach walking reconsidered: discharges of proximal tibial campaniform sensilla when body load is altered *J. Comp. Physiol.* A **187** 769–84

Noah J A, Quimby L, Frazier S F and Zill S N 2004 Sensing the effect of body load in legs: responses of tibial campaniform sensilla to forces applied to the thorax in freely standing cockroaches *J. Comp. Physiol.* A **190** 201–15

Pearson K G 1972 Central programming and reflex control of walking in the cockroach *J. Exp. Biol.* **56** 173–93

Prilutsky B I, Klishko A N, Weber D J and Lemay M A 2016 Computing motion dependent afferent activity during cat locomotion using a forward dynamics musculoskeletal model *Neuromechanical Modeling of Posture and Locomotion* ed ed B I Prilutsky and D H Edwards (New York: Springer) pp 273–307

Prochazka A, Gillard D and Bennett D J 1997a Implications of positive feedback in the control of movement *J. Neurophysiol.* **77** 3237–51

Prochazka A, Gillard D and Bennett D J 1997b Positive force feedback control of muscles *J. Neurophysiol.* **77** 3226–36

Prochazka A and Gorassini M 1998 Models of ensemble firing of muscle spindle afferents recorded during normal locomotion in cats *J. Physiol.* **507** 277–91

Ridgel A L, Frazier S F, Dicaprio R A and Zill S N 1999 Active signaling of leg loading and unloading in the cockroach. *J. Neurophysiol.* **81** 1432–7

Ridgel A L, Frazier S F, DiCaprio R A and Zill S N 2000 Encoding of forces by cockroach tibial campaniform sensilla: implications in dynamic control of posture and locomotion *J. Comp. Physiol.* A **186** 359–74

Ridgel A, Frazier F and Zill S 2001 Dynamic responses of tibial campaniform sensilla studied by substrate displacement in freely moving cockroaches *J. Comp. Physiol.* A **187** 405–20

Sandbrink K J, Mamidanna P, Michaelis C, Mathis M W, Bethge M and Mathis A 2020 Task-driven hierarchical deep neural network models of the proprioceptive pathway 10.1101/2020.05.06.081372 (Retrieved from bioRxiv on 26 May 2020)

Sutton G, Szczecinski N, Quinn R and Chiel H 2021 Neural control of rhythmic limb motion is shaped by size and speed 10.21203/rs.3.rs-153297/v1 (Retrieved from Research Square on 20 August 2021)

Szczecinski N S *et al* 2015 Introducing MantisBot: hexapod robot controlled by a high-fidelity, real-time neural simulation *IEEE Int. Conf. Intelligent Robots and Systems* (Hamburg, DE) pp 3875–81

Szczecinski N S, Getsy A P, Martin J P, Ritzmann R E and Quinn R D 2017 MantisBot is a robotic model of visually guided motion in the praying Mantis *Arthropod Struct. Dev.* **46** 736–51

Szczecinski N S and Quinn R D 2017 Leg-local neural mechanisms for searching and learning enhance robotic locomotion *Biol. Cybern.* **112** 99–112

Szczecinski N S, Quinn R D and Hunt A J 2020 Extending the functional subnetwork approach to a generalized linear integrate-and-fire neuron model *Front. Neurorob.* **14** 577804

Szczecinski N S, Zill S N, Dallmann C J and Quinn R D 2020 Modeling the dynamic sensory discharges of insect campaniform sensilla *Conf. Biomimetic and Biohybrid Systems* pp 342–53

Thorson J and Biederman-Thorson M 1974 Distributed relaxation processes in sensory adaptation: spatial nonuniformity in receptors can explain both the curious dynamics and logarithmic statics of adaptation *Science* **183** 161–72

Torkkeli P H and French A S 2002 Simulation of different firing patterns in paired spider mechanoreceptor neurons: the role of Na^+ channel inactivation *J. Neurophysiol.* **87** 1363–8

Tuthill J C and Wilson R I 2016 Mechanosensation and adaptive motor control in insects *Curr. Biol.* **26** 1022R–38

Witte H *et al* 2002 Torque patterns of the limbs of small therian mammals during locomotion on flat ground. *J. Exp. Biol.* **205** 1339–53

Zill S N, Büschges A and Schmitz J 2011 Encoding of force increases and decreases by tibial campaniform sensilla in the stick insect, carausius morosus *J. Comp. Physiol.* A **197** 851–67

Zill S N, Chaudhry S, Büschges A and Schmitz J 2015 Force feedback reinforces muscle synergies in insect legs *Arthropod Struct. Dev.* **44** 1–13

Zill S N, Chaudhry S, Exter A, Büschges A and Schmitz J 2014 Positive force feedback in development of substrate grip in the stick insect tarsus *Arthropod Struct. Dev.* **43** 441–55

Zill S N, Dallmann C J, Büschges A, Chaudhry S and Schmitz J 2018 Force dynamics and synergist muscle activation in stick insects: the effects of using joint torques as mechanical stimuli *J. Neurophysiol.* **120** 1807–23

Zill S N, Dallmann C J, Szczecinski N S, Büschges A and Schmitz J 2021 Evaluation of force feedback in walking using joint torques as 'naturalistic' stimuli *J. Neurophysiol.* **126** 227–48

Zill S N, Frazier S F, Lankenau J and Jepson-Innes K 1992 Characteristics of dynamic postural reactions in the locust hindleg *J. Comp. Physiol.* A **170** 761–72

Zill S N, Keller B R and Duke E R 2009 Sensory signals of unloading in one leg follow stance onset in another leg: transfer of load and emergent coordination in cockroach walking *J. Neurophysiol.* **101** 2297–304

Zill S N and Moran D T 1981a The exoskeleton and insect proprioception: I. Responses of tibial campaniform sensilla to external and muscle-generated forces in the American cockroach, periplaneta americana *J. Exp. Biol.* **91** 1–24

Zill S N and Moran D T 1981b The exoskeleton and insect proprioception: III. Activity of tibial campaniform sensilla during walking in the American cockroach, periplaneta americana *J. Exp. Biol.* 57–75

Zill S N, Schmitz J, Chaudhry S and Büschges A 2012 Force encoding in stick insect legs delineates a reference frame for motor control. *J. Neurophysiol.* **108** 1453–72

Zill S, Schmitz J and Büschges A 2004 Load sensing and control of posture and locomotion *Arthropod Struct. Dev.* **33** 273–86